Microchimica Acta (2022) 189: 213
https://doi.org/10.1007/s00604-022-05301-w

ORIGINAL PAPER

A ratiometric electrochemical DNA-biosensor for detection of miR-141

Ali Khodadoust[1] · Navid Nasirizadeh[2] · Ramezan Ali Taheri[3] · Mohammad Dehghani[2] · Mostafa Ghanei[4] · Hasan Bagheri[4]

Received: 27 December 2021 / Accepted: 30 March 2022 / Published online: 5 May 2022

Abstract

A sensitive biosensor for the detection of miR-141 has been constructed. The DNA-biosensor is prepared by first immobilizing the thiolated methylene blue-labeled hairpin capture probe (MB-HCP) on two-layer nanocomposite film graphene oxide-chitosan@ polyvinylpyrrolidone-gold nanourchin modified glassy carbon electrode. We used the hematoxylin as an electrochemical auxiliary indicator in the second stage to recognize DNA hybridization via the square wave voltammetry (SWV) responses that record the accumulated hematoxylin on electrode surfaces. The morphology and chemical composition of nanocomposite was characterized using TEM, FE-SEM, and FT-IR techniques. The preparation stages of the DNA-biosensor were screened by electrochemical impedance spectroscopy and cyclic voltammetry. The proposed DNA-biosensor can distinguish miR-141 from a non-complementary and mismatch sequence. A detection limit of 0.94 fM and a linear range of 2.0 –5.0 × 10^5 fM were obtained using SWV for miR-141 detection. The working potential for methylene blue and hematoxylin was -0.28 and + 0.15 V *vs.* Ag/AgCl, respectively. The developed biosensor can be successfully used in the early detection of non-small cell lung cancer (NSCLC) by directly measuring miR-141 in human plasma samples. This novel DNA-biosensor is of promise in early sensitive clinical diagnosis of cancers with miR-141 as its biomarker.

Keywords Biosensor · miR-141 · Early Detection · Lung Cancer · Electrochemical biosensors

Introduction

Lung cancer (pulmonary carcinoma) is the first most common cancer with the highest mortality rate worldwide (1.7 million/year) [1]. Lung cancer can be detected through the cancer biomarkers such as blood-based miRNAs which are considerably resistant to RNase activity, extreme temperature, and pH [2]. Also, they are extremely stable and easily extracted and can be reliably evaluated in patient samples via a non-invasive manner [3].

In non-small cell lung cancer (NSCLC) cells, miR-141 has been reported to promote proliferation by regulation of pH domain leucine-rich-repeats protein phosphatase 1, 2 (PHLPP1, PHLPP2), and KLF9 [4]. The miR-141 in lung cancer serum and tissue is overexpressed and associated with overall survival. However, the role of plasma miR-141 expression in prognosis and diagnosis of NSCLC patients is still not clear. Therefore, the detection of miR-141 in an early stage of lung cancer has great importance. Diagnostically, the level of miR-141 in plasma can provide information about tumor initiation, invasion, and metastasis processes [5, 6].

Numerous nanostructures with unique features have been used to improve the sensitivity of biosensors via increasing the surface area, including in electrochemical biosensors to detect miRNAs, especially for lung cancer [7–10].

Graphene oxide (GO), made by the oxidation of graphite using strong oxidizing agents, is cheaper than graphene and has unique features including: high-affinity conjugation with the biocomponent molecules and increased aqueous or organic solvents dispersibility caused by covalently bounded oxygen groups that make it an appropriate platform

✉ Hasan Bagheri
h.bagheri@bmsu.ac.ir; h.bagheri82@gmail.com

1 Applied Biotechnology Research Center, Baqiyatallah University of Medical Sciences, Tehran, Iran

2 Department of Textile and Polymer Engineering, Yazd Branch, Islamic Azad University, Yazd, Iran

3 Nanobiotechnology Research Center, Baqiyatallah University of Medical Sciences, Tehran, Iran

4 Chemical Injuries Research Center, Systems Biology and Poisonings Institute, Baqiyatallah University of Medical Sciences, Tehran, Iran

for further chemical modifications [11–14]. Chitosan (CS) is a cationic biomacromolecule, which has high adhesion and high film-forming capability via its primary amines. By adopting CS, the reproducibility, homogeneity, and dispersion of graphene can be improved and enhanced the stability of the biosensor [15]. Nowadays appealing substances similar to conductive electroactive polymers (CEPs) have been much used to improve the electrode surface of biosensors. Among them, polyvinylpyrrolidone (PVP), a water-soluble neutral non-toxic/ionic promising CEPs, exhibits an intense affinity to metal nanoparticles such as gold and silver due to its hydrophobic (polyvinyl) and hydrophilic (pyrrolidone) groups [16]. PVP also avoids the agglomeration of NPs due to its significant stabilizing role [17]. Nanoparticles/PVP such as AuNPs/PVP, AgNPs/PVP, and GO/PVP are considered as high catalytic electroactive and long-term stable nanocomposite in new platforms (e.g., nanofiber, nanofilm, hydrogel, etc.) in electrochemical nanobiosensors [18–20].

In this work, we constructed an electrochemical biosensor with an operational thiolated hairpin probe on the basis of two layers' nanocomposite (GO-CS/PVP-Au) film to measure miR-141 for the early detection of lung cancer. A GO-CS/PVP-AuNUs nanocomposite film-modified glassy carbon electrode (GCE/GO-CS/PVP-AuNUs) was used as a high steaky stable and conductive substrate to immobilize a thiolated probe.

In addition to methylene blue as the main label, we also used hematoxylin (HEM) as a helper electrochemical indicator to be able to measure the amount of hybridization as well as the biosensor detection accuracy. To the best of our knowledge, AuNU/PVP/CS-GO nanocomposite has never been used in any electrochemical biosensors for miR-141 detection.

Experimental Section

Oligos and chemicals

The sequence of oligos and composition of the solutions are described in Electronic Supporting Material (ESM), Sect. 1 and Table S1.

Instruments and electrochemical measurements

Electrochemical experiments, including cyclic voltammetry (CV), square wave voltammetry (SWV), and electrochemical impedance spectroscopy (EIS), were done using three-electrode system containing a working electrode (modified GCE), an Ag/AgCl electrode as the reference electrode, and an auxiliary electrode (platinum electrode). The procedure of experiments is described in ESM, Sect. 2.

Preparation of two-layer nanocomposite film electrode

The synthesis procedures of GO-CS nanocomposite, polyvinylpyrrolidone-gold nanourchin (PVP-AuNUs) nanocomposite and the process of two-layer nanocomposite preparation are completely explained in ESM, Sects. 3 to 5.

Hairpin probe immobilization and hybridization

In the first, the disulfide bonds of the MB-HCP were reduced using dithiothreitol (DTT) according to the method of Tang et al. 2019 [3]. The capture probe was treated in a bain-marie of 85°C for 25 min and ice-cold water for 15 min to prevent the formation of dipolymer. Then, the capture probe (0.6 µM final concentration) was diluted in immobilization buffer (25.0 mM Tris–HCl, 100.0 mM $MgCl_2$, 100.0 mM NaCl, pH 8.0) and 15 µL of the solution was meticulously placed onto the surface of GCE/GO-CS/PVP-AuNUs and incubated for 16 h at 4°°C and the electrode was covered with a plastic cap to avoid evaporation of the solution. After thorough washing with the washing solution (10.0 mM Tris–HCl, pH 8.0), the electrode was submerged in 1.0 mM MCH solution for 30 min to remove non-specific adsorption of the probe as well block the remaining naked areas on the surface of AuNUs. After rinsing with washing solution, the ready electrode was submerged in the hybridization buffer (10.0 mM Tris–HCl, 25.0 mM NaCl, pH 8.0) containing different concentrations of the anti-miR-141 capture probe (ACP-141) at 37°°C for 120 min [21, 22]. Finally, the DNA-biosensor was ready after extensive rinsing with washing buffer. EIS and CV analysis was performed to confirm the electrode modifications.

HEM accumulation on the DNA-biosensor.

In order to create a control, prepared biosensor was submerged in the 0.1 mM PBS (pH 8.0) containing 0.1 mM of HEM for 10-min stirring at 100 rpm speeds without applying the miR-141 samples followed by rinsing with a washing solution for 10 s. Scheme 1 illustrates the fabrication steps of the proposed biosensor.

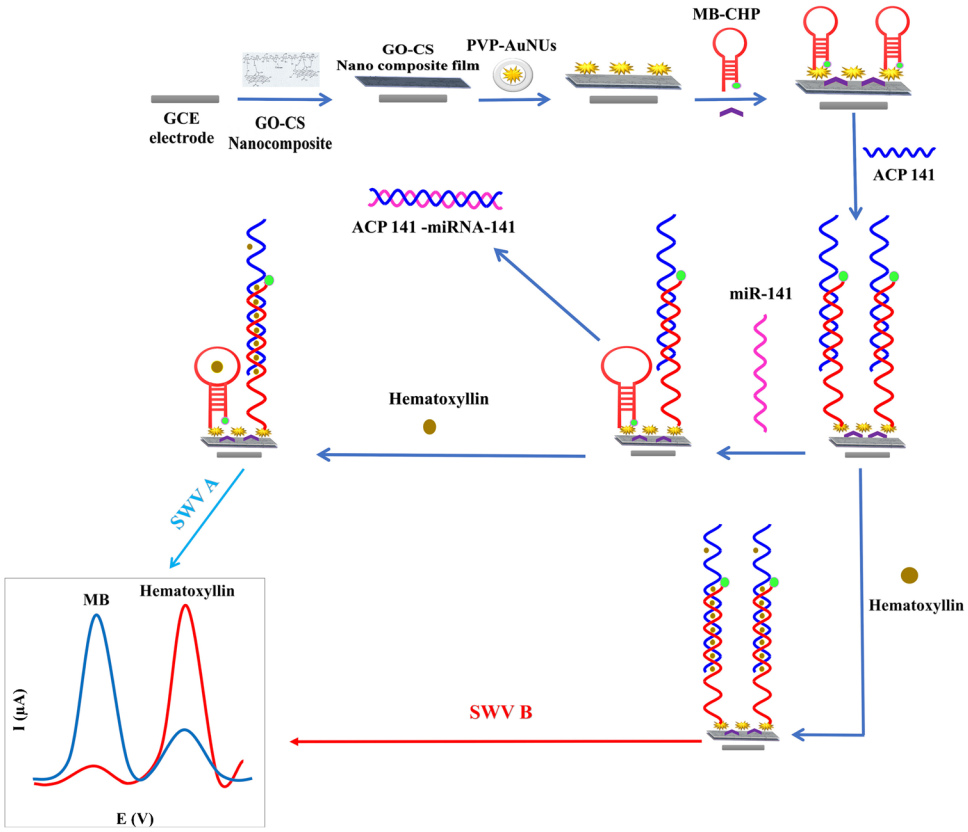

Scheme 1 Schematic representation of construction process of DNA-biosensor

Preparation of samples

Due to the significant role of early monitoring and detection in lung cancer treatment [23], the proposed DNA-biosensor was used to measure miR-141 in the blood plasma samples. For this purpose, a healthy non-cancerous human blood plasma was provided from the Bio Bank of Shiraz University of Medical Sciences. The applicability of developed device is evaluated at the beginning of the whole analytical process, via incubation of the prepared DNA-biosensor (in a humid chamber for 120 min at 37 °C) in undiluted blank and containing 0.1 nM miR-141 plasma samples (2.0 µL of 500 pM miR-141 solution was taken to a final volume of 10 µL with human undiluted plasma sample). Since the concentration of miR-141 in the non-cancerous plasma, like other miRNAs, is at very low or undetectable levels, less than the detection limit of the prepared DNA-biosensor (Fig. 1) [24], the primary concentration of miR-141 in the plasma sample was lower than detection limit of the method [23, 24] and therefore, different concentrations of miR-141 were spiked into tenfold diluted plasma sample (with RNase-free phosphate buffer).

Results and Discussion

The main mechanism is based on detachment of the anti-miR-141 capture probe (ACP-141) in the presence of the miR-141 (Scheme 1). The thiolated capture hairpin probe (MB-CHP) is self-assembled on the GCE after modification of the electrode with two layers' nanocomposite GO-CS and AuNUs film and then partially hybridized with ACP-141. After the introduction of miR-141, the partially hybridization of MB-CHP with a segment of ACP-141 and also the more tendency of this probe (ACP-141) toward its specific miRNA (miR-141), makes the anti-miR-141 capture probe detached from MB-CHP. Thus, the SWV signal of the electrochemical label, methylene blue (MB), increases and the SWV signal of HEM decreases. The results of research on the mechanism of action of HEM with DNA show that the intercalation and electrostatic binding are the two major modes for interaction between HEM and DNA [25–27]. According to the previous publications of our research team the signal of the HEM accumulated on single-stranded DNA (ssDNA)/electrode is smaller than that of double-stranded DNA (ds-DNA)/electrode. This indicates that the interaction of HEM with ds-DNA is stronger than ss-DNA [8, 25].

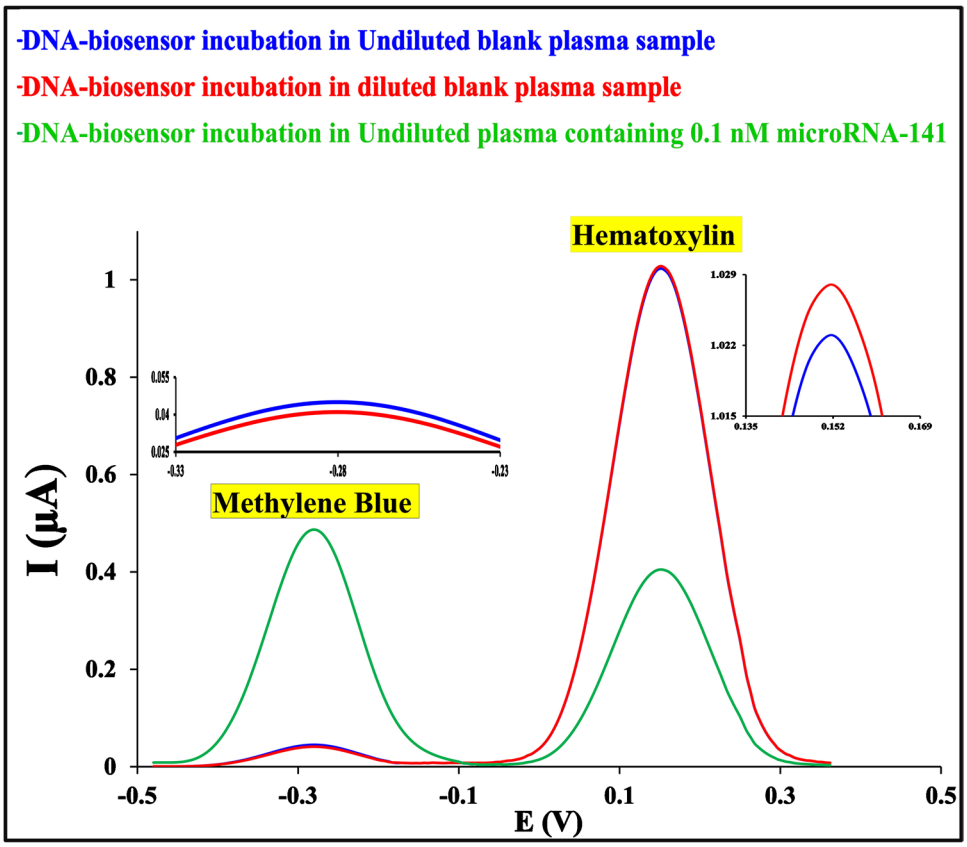

Fig. 1 Typical SWV responses during DNA-biosensor incubation in undiluted blank plasma sample, incubation in diluted blank plasma sample, and incubation in undiluted plasma containing 0.1 nM miR-141. All the SWV data were collected in potentials ranging from -0.5 V to 0.5 V *vs.* Ag/AgCl, and the supporting electrolyte is 0.1 M KCl

Therefore, the presence of miR-141 reduces the HEM signal and increases the MB-CHP signal.

Unlike the single reported bioassays, the ratiometric dual-signal strategy is more effective and reliable because it reduces external interferences and provides a more accurate signal, due to its features in the significant elimination of false-positive errors by the built-in correction mechanism as well as the ability of ratiometrically increasing the detection signal as a major amplification approach at the relatively low concentration. Therefore, the ratiometric dual-signal method has the merits of high sensitivity and selectivity, excellent accuracy, and good stability [28, 29].

Characterization of electrode surface

The field-emission SEM and TEM were performed using a Zeiss EVO MF10 scanning electron microscope and a Zeiss-EM10C transmission electron microscope (Germany), respectively, to portray the morphologies of electrode surface after modification with the first (CS-GO) and second (GO-CS/PVP-AuNUs) layers of nanocomposite film, respectively. As shown in Fig. 2A, first-layer nanocomposite (CS-GO) displayed the unevenly corrugated and crumpled sheet-like structures, which could extend the surface area, dispersibility, and also adhesion on the electrode surface effectively [28, 30]. After that, the composition of chemo-polymerized vinylpyrrolidone (PVP) as a capping agent with gold nanomaterials has a significant effect in the regular shape formation of stabilized AuNUs (e.g., cubes, wires) and also prevents their agglomeration on electrode surface [31], (Figs. 2B, C, D). The high-magnification TEM image in Fig. 2E shows spherical-shaped AuNUs with diameter of ~ 14 ± 2 nm, settled on the top of film. FTIR spectra were used to investigate the successful synthetic process of nanocomposite film (Section S6 and Fig. S1). This well-proportioned two-layer nanocomposite film structure (GO-CS/PVP-AuNUs) could remarkably enhance the electrode-efficient surface area and increase the electron transfer ability and also the probe loading amount.

Electrochemical characterization of the miR-141 DNA-biosensor

The electrochemical behavior of the DNA-biosensor was investigated after each preparation step by using EIS and CV methods. EIS is a notable and appropriate technique for monitoring the impedance changes of surface-modified transfer electrodes. In the Nyquist plot, the semicircle diameters at high-frequency region indicate the electron transfer resistance (R_{et}) which controls the electron transfer kinetics

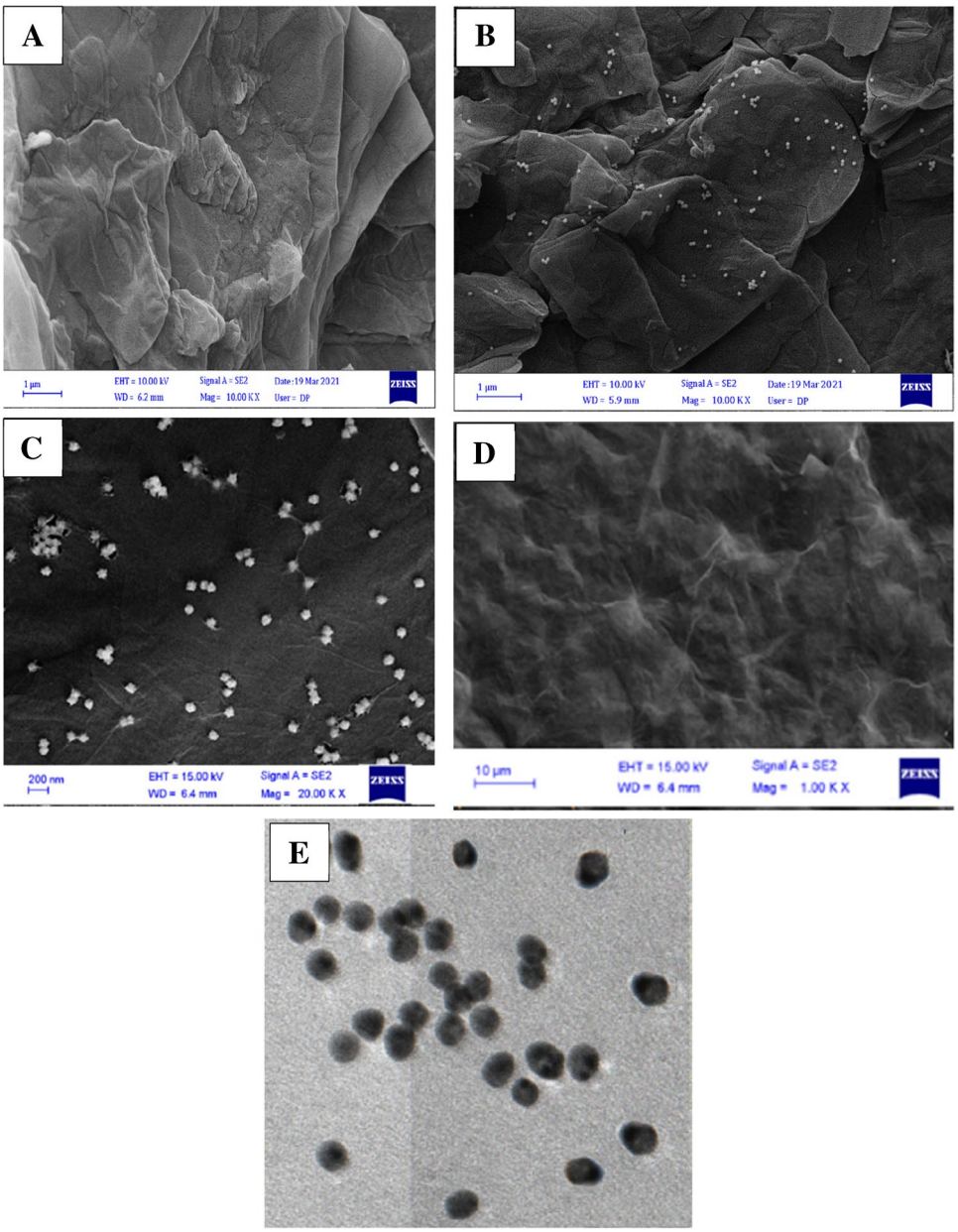

Fig. 2 FESEM images of the CS-GO (A) and GO-CS/PVP-AuNUs (B, C, D) modified GC electrode. (E) TEM image of GO-CS/PVP-AuNUs/GCE

of the redox probe at the electrode interface [22, 32]. In these plots the diameter of the semicircular is related to the R_{et} and the linear region demonstrates a diffusion limited process [30]. As it is illustrated in Fig. 3A, the AuNU-PVP/CS-GO modified GCE (pink) exhibited an approximately straight line (87 Ω), while the R_{et} of bare GCE was 625 Ω (Black), which clearly exhibited the great electron-transfer superiority of our method [33]. After immobilization of CHP, the R_{et} value enhanced to 0.94 KΩ, because of the assembling of negatively charged phosphoric acid backbones of DNA probe which repelled the $[Fe(CN)_6]^{3-/4-}$ and inhibited the electron transfer (Red) [22]. The resistance value significantly raised to 1.9 KΩ and 3.58 KΩ (brown and green curves) after the electrode sealed with MCH and ACP-141, respectively. This was due to the blocking of MCH with non-conductive properties and a large amount of negatively charged phosphoric acid backbones as a result of dsDNA formation [34], elucidating that DNA hybridization was approvingly situated onto the electrode, respectively. In addition, the R_{et} value decreased to 2.82 KΩ (blue curve) when miR-141 attached onto the ACP-141, and this decrease was the obvious evidence of prosperous binding of CHP onto the electrode surface due to attaching of target miRNA onto ACP-141. The EIS analysis of different modified electrodes before the construction of biosensor is exhibited in Fig. 3B. As it can be observed, the GCE has a low electron transfer resistance. After the modification of GCE with the GO-CS/PVP-AuNUs nanocomposite film, the

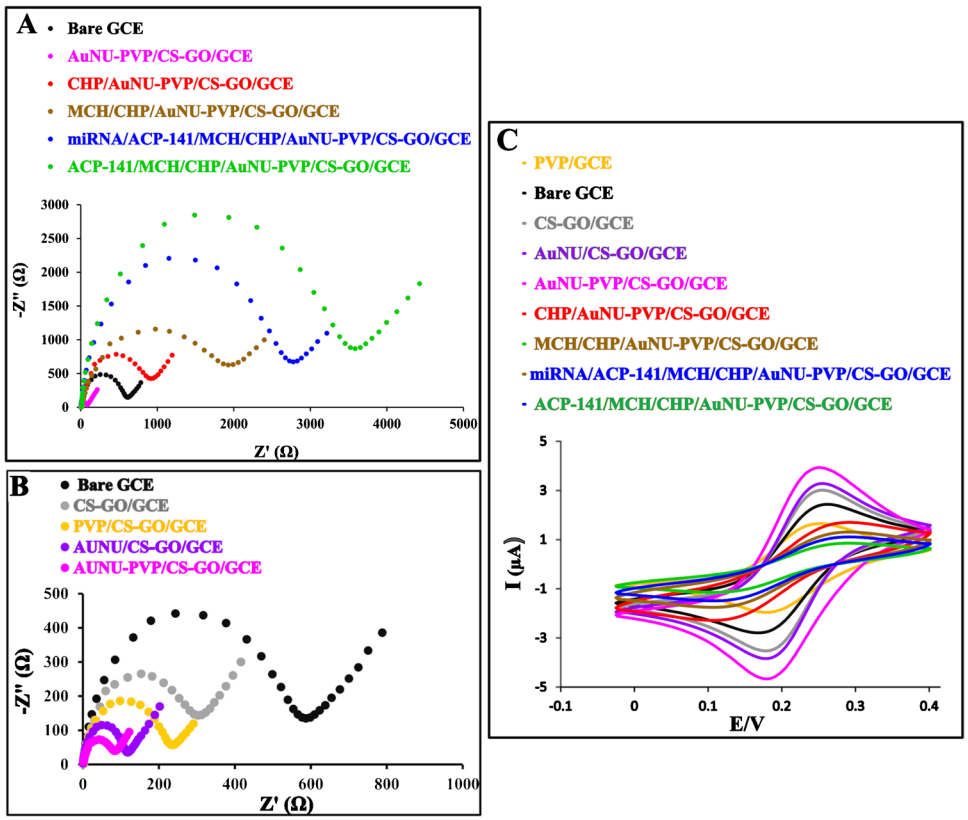

Fig. 3 Electrochemical impedance spectra of each immobilization step (A) for surface modifications (B) of DNA-biosensor. (C) Characterization of GCE after each step of surface modification and immobilization by CV measurements in 0.1 M KCl aqueous solution containing 5.0 mM $[Fe(CN)_6]^{3-/4-}$ as redox species, scan rate: 20 mV/s

diameter of the semicircle decreased. This was due to the excellent conductivity of the two-layer nanocomposite film which increased the electron transfer, hence reducing the surface resistance between the redox probe and the modified electrode [22, 35].

Modification processes were evaluated using CV. As shown in Fig. 3C, there was a clear reduction in voltammetric signal after PVP modified onto the electrode (Yellow) compared with bare GCE (black), denoting that PVP itself was not conductive. However, the peak currents increased slightly after AuNUs (purple) onto the first layer of nanocomposite film (gray), but the peak current remarkably raised (pink) after the chemical deposition of AuNUs onto the GCE/GO-CS/PVP surface, which could effectually amplify the electron transfer rate and magnify the immobilizing amount of hairpin probes. The effect of CHP immobilization and the addition of MCH, ACP-141 as well as miR-141 on the rate of current reduction due to the increase in resistance value are also shown in Fig. 3C.

Optimization of the experimental conditions

This section is explained in ESM, Sect. 7.

Analytical performance of the biosensor

The HEM employed as an auxiliary indicator in our novel approach design, is a stain that exhibits a stronger priority for double-stranded DNA (dsDNA) than ssDNA and self-assembled DNAs such as hairpin probes [16, 34]. The thiol modified CHP labeled with MB (MB) tag is self-assembled on the modified glassy carbon electrode surface (GCE/GO-CS/PVP-AuNUs) via the formation of Au – S bonds [36]. Subsequent surface blocking with MCH and then hybridization with the complementary miR-141 probe lead to the preparation of the sensor by the unfolding of the MB-HCP to form DNA/DNA duplexes, which are perfect substrates for HEM [22, 32]. In the absence of the target miRNA (miR-141), a significant current peak (HEM: + 0.15 V) can thus be expected with the addition of HEM, because of the intercalation mechanism of HEM-DNA interaction and efficient electron transfer between the HEM and the sensor surface [34]. The anti-miR-141 capture probe (ACP-141) releases after the target miRNA (miR-141) is incubated with the DNA-biosensor and the CHP is formed again. Less preference of HEM to the self-assembled CHP than dsDNA leads to highly suppressed current peak at HEM potential position (+ 0.15 V) and a sharp increase in current peak of MB (-0.28 V).

We first display the susceptibility of DNA-biosensor for the detection of miR-141 with the addition of HEM. As shown in Fig. 4A, in the absence of the target miRNA, the sensor exhibits a sharp current peak at potential position of HEM at + 0.15 V. Due to electrochemical oxidation of the HEM, the incubation of the target miR-141 with the sensor leads to notable increase in current response at − 0.28 V, while the peak corresponding to HEM at 0.15 V is reduced (Fig. 4, B *vs.* A).

As displayed in Fig. 5A, the current responses of HEM and MB redox tag can be decreased and increased, respectively, with increased concentration of the target miRNA and the ratio of I_{MB}/I_{HEM} was used for miR-141 analysis. The calibration plots of MB and HEM as well as the calibration curve of the I_{MB}/I_{HEM} values against the logarithm of miR-141 concentration are shown in Fig. 5B-D. The corresponding linear regression equation and a correlation coefficient ($R^2 = 0/9941$) of I_{MB}/I_{HEM} are better than I_{MB} or I_{HEM}. A linear relationship was obtained in the range from 2.0×10^{-3} – 500.0 pM (a to f in Fig. 5A), and the limit of detection (LOD) was 0.94 fM (N = 3). Obviously, as shown in Fig. 5, the proposed ratiometric strategy based on I_{MB}/I_{HEM} possessed the premier analytical performance than that based on individual I_{MB} or I_{HEM} signal. Individual signal of I_{HEM} and I_{MB} as the response exhibits a linear relationship in the ranges of 5.0×10^{-3} – 70.0 pM and 7.0×10^{-3} – 100.0 pM along with the detection limits of 1.67 and 1.12 fM, respectively, using the equation LODs = 3.3 S_B/m [37], where S_B is the standard deviation of the mean value from the linear regression of calibration curve of low concentrations of the target (the ratio signal of MB /HEM at ds-DNA/GCE) and m is the slope of the calibration plot. Table 1 indicates the analytical information for developed biosensors for detection of miR-141. As illustrated, electroluminescence and photoelectrochemical methods have been used, which have the ability to identify the studied biomarkers in very low concentrations, but have a complicated and expensive design. However, interfering factors and noises can influence on the measurement process. The proposed method in this study is an electrochemical method based on voltammetry and impedance that has a simple and user-friendly design. Here, a ratiometric mechanism is used to receive the signal, which acts as a preprocessor to remove the interferences and increases the selectivity of the sensor. Also, the detection limit of the proposed method is comparable to previous reports.

Selectivity, reproducibility, repeatability, regeneration and stability of the biosensor

The selectivity of the DNA-biosensor was evaluated for the recognition of the target from other miRNA sequences. For this purpose, the ACP-141/MCH/MB-HCP/AuNUs-PVP/GO-CS/GCE was hybridized with a non-complementary sequence, a two-base mismatch sequence, and a complementary sequence (miR-141). Then, the electrochemical responses of two indicators on the modified electrode surface were recorded. Figure 5. E shows the SWV of (a) the prepared biosensor after hybridization with (b) a non-complementary sequence (miR-103a), (c) a four-base mismatched (miR-200b), each at a concentration of 0.1 nM, and (d) a target RNA sequence (miR-141) at a concentration of 7.0 pM. As the figure suggests, the greatest and the

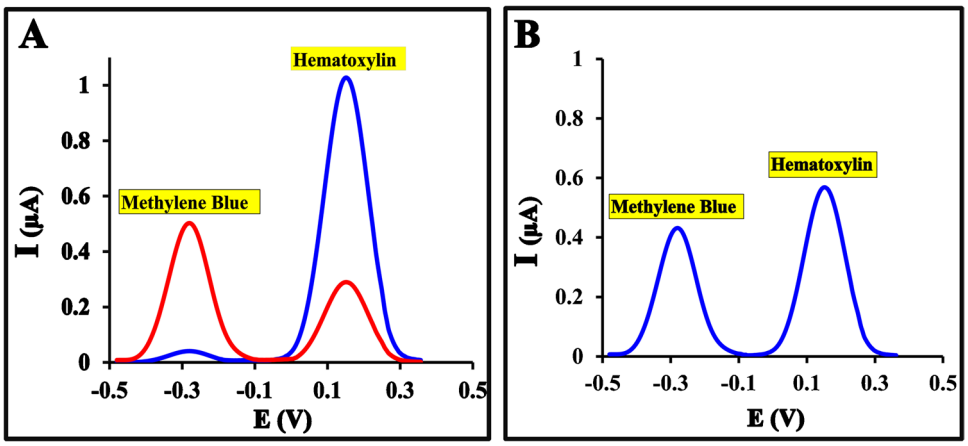

Fig. 4 (A) Typical SWV responses during DNA-biosensor fabrication steps in the optimized condition: after immobilization of thiolated methylene blue-labeled hairpin capture probe (MB-HCP) on the electrode (red curve) and after its hybridization with ACP-141 (Anti-miR-141 capture probe) in the final step (blue curve), (B) SWV responses of prepared DNA-biosensor after incubation (120 min at 37 °C) with miR-141 (7.0 pM). SWV measurements were taken in a 0.1 M PBS at pH 8.0 buffer with a frequency of 25 HZ, a step potential of 4 mV, and an amplitude of 25 mV

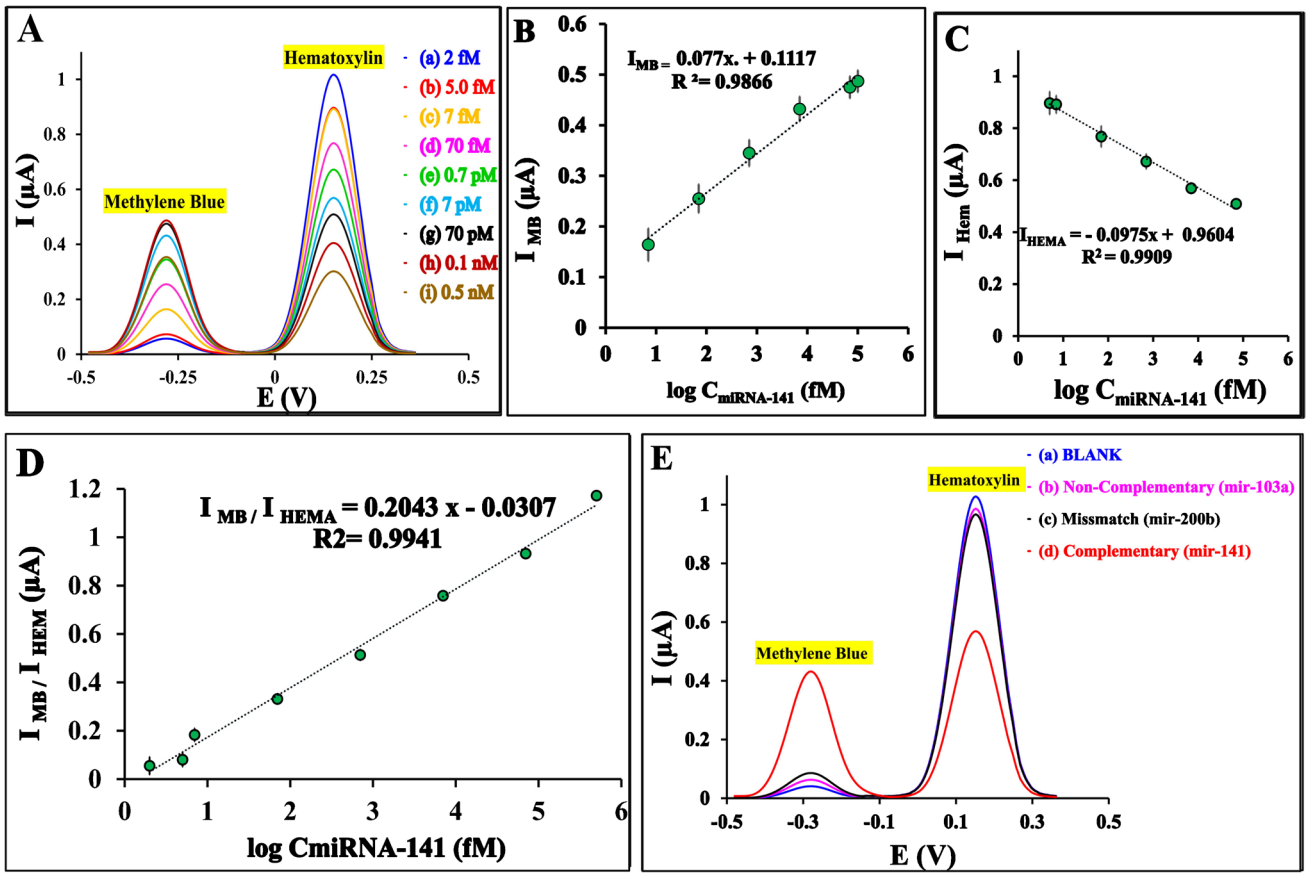

Fig. 5 (A) Typical SWV responses of the proposed sensor for multiplexed detection of miR-141 after incubation (120 min at 37 °C) at: (a) 2 fM, (b) 5.0 fM, (c) 7 fM, (d) 70 fM, (e) 0.7 pM, (f) 7 pM, (g) 70 pM, (h) 0.1 µM, (i) 0.5 µM, and the calibration curve for miR-141 determination by individual (B) I_{MB}, (C) I_{HEM}, and the ratio of I_{MB}/I_{HEM} (D), as the response. (E) Specificity investigation of the sensor for the target miR-141 (7.0 pM) against other control sequences of miR-200b (0.1 nM) and miR-103a (0.1 nM), respectively. SWV measurements were taken in a 0.1 M PBS at pH 8.0 with a frequency of 25 HZ, a step potential of 4 mV, and an amplitude of 25 mV (the working potential for MB and HEM was -0.28 and + 0.15 V *vs.* Ag/AgCl, respectively)

smallest peak currents of the MB and the accumulated HEM, respectively, occurred after the incubation of the ACP-141/MCH/MB-HCP/AuNUs-PVP/GO-CS/GCE with the target miRNA rather than the mismatch and non-complementary sequences. Moreover, the large difference between the responses of the d and a voltammograms demonstrates that simultaneous use of our two selected indicators as an electrochemical label can provide excellent discrimination ability, and the prepared biosensor has satisfactory selectivity for the detection of miR-141 and, thus, be applied for the analysis of miR-141 in biomicroenvironments.

The reproducibility was assessed by four parallel measurements of 7 pM miR-141 on different days in the same batch and two laboratories. The relative standard deviation (RSD) was estimated to be 4.91%, demonstrating its acceptable reproducibility for laboratory-scale production. The repeatability is also another key factor in assessing the accuracy and evaluated for the concentration of 7.0 pM miR-141 in 7 repeated measurements. The relative standard deviation (RSD) was found to be 3.7%.

The reusability of the DNA-biosensor is considerably significant for practical application, such as biological and clinical diagnoses, which is dependent on the regeneration ability and stability of the biosensor [38]. Surface of the prepared DNA-biosensor was incubated in hot water (80 ℃) for 5 min and then washed several times with deionized water. The DNA-biosensor retained 97.2% of its origin current response after five cycles of regeneration. The signal response of miR-141 reached 91.7% of the initial value after storing of the proposed DNA-biosensor at 4 °C for 20 days. This high rigidity can be ascribed to the great chemical and environmental stability of PVP [16]. Furthermore the anti-interference evaluation of the DNA-biosensor for some different kinds of other control species including tetracycline, ascorbic acid, albumin and ca^{2+} was examined. As shown in Fig. S3, the I_{MB} / I_{Hem} SWV signal response of the miR-141

Table 1 Comparison of the DNA-biosensor parameters and functions with previous publications for miR-141 detection

Method	LOD	Linear Range	Ref
ECL	31.9 aM	100 aM–0.1 nM	[41]
Photoelectrochemical	2.4 aM	0.1 fM to 1 nM	[42]
Electrochemical (SWV)	3.23 aM	10 aM to 10 pM	[43]
Photoelectrochemical	0.33 fM	1 fM to 1 nM	[44]
Photoelectrochemical	0.3 fM	1 fM to 1 nM	[45]
Fluorescence	0.088 nM	0.1 – 50 nM	[46]
Fluorescence	0.001 nM	0.001 - 5 nM	[47]
Chemiluminescence	0.1 nM	0.1 - 50 nM	[48]
Chemiluminescence	280 fM	----	[49]
Mass spectrometry	42 pM	----	[50]
Mass spectrometry	10 fM	----	[51]
Surface Enhanced Raman Spectroscopy (SERS)	<0.01 pM	1 - 10000 pM	[52]
Electrochemical (SWV)	0.08 pM	0.01–100 pM	[53]
Electrochemical (SWV)	0.01 pM	0.01 - 1000 pM	[54]
Electrochemical	10^{-6}µM	10^{-6} - 100 µM	[55]
Electrochemical	10 pM	50 - 1000 pM	[56]
Electrochemical	138 aM	500 aM–50 nM	[57]
Ratiometric electrochemical SWV	0.94 fM	2.0 fm – 0.5 nM	This Work

sample was much higher than those of other interfering substances, indicating that the prepared ratiometric biosensor has better specificity and selectivity toward miR-141.

Determination of miR-141 in human plasma samples

Comparison of the SWV responses of the DNA-biosensor after incubation in undiluted blank plasma (0.045 ± 0.002 µA for MB and 1.023 ± 0.001 µA for Hem) with diluted blank plasma sample (0.041 ± 0.001 µA for MB and 1.028 ± 0.002 µA for Hem) indicates that the blank plasma sample has no effect on the electrochemical response of the DNA-biosensor (Fig. 1). However, after incubation of the DNA-biosensor in undiluted plasma sample containing 0.1 nM microRNA-141, the reduction peaks of the accumulated MB and HEM dramatically decrease and increase, respectively. This indicates that the DNA-biosensor is suitable for detection of miR-141 in the human plasma sample. The accuracy of the biosensor was further assessed by recovery assay. In the first, the initial concentration of miR-141 was detected using a qRT-PCR. Subsequently, miR-141 solutions of different concentrations (10 fM to 10 pM) can be obtained by diluting the initial miR-141 solution. In total, 10 µl of the prepared solutions was incubated on the ACP-141/MCH/MB-HCP/AuNUs-PVP/GO-CS/GCE, and the SWV of the accumulated MB and HEM was recorded. Then, the recovery rates of the prepared samples were calculated. To evaluate method reliability, the qRT-PCR [39, 40] was also used as a gold-standard method for analysis of initial concentration of miR-141 in human plasma samples. The results are summarized in Table 2. As the table suggests, the proposed DNA-biosensor can be employed to measure miR-141 in clinical samples.

Table 2 Recovery results corresponding to miR-141 determination in a human plasma sample (N = 4) using the proposed DNA-biosensor

Samples	Spiked (fM $10\mu L^{-1}$)	Developed Method			qRT-PCR	
		Detected (fM $10\mu L^{-1}$)	Recovery (%)	RSD (%)	Detected (Copy number $10\mu L^{-1}$)	Recovery (%)
Human Plasma	0.0	-	-	-	83 – 176 ~ 0.1 – 0.3 fM/10ul	-
	10	10.47	104.7	5.3	61.0×10^{8} ~ 10.13 fM/10ul	101.3
	100	99.0	99.0	4.2	58.79×10^{9} ~ 97.63 fM/10ul	97.63
	10,000	9690	96.9	4.6	533.1×10^{10} ~ 8851 fM/10ul	88.51

Conclusion

An electrochemical DNA-biosensor was constructed for measuring miR-141 in the early stages of lung cancer. To this end, AuNUs-PVP/GO-CS was used as an excellent substrate with high conductivity to immobilize a thiolated probe on the surface of a GCE. In addition, MB served as an electroactive label and HEM as an auxiliary indicator. The results showed that HEM as auxiliary indicator has more interaction with dsDNA than ssDNA. Through SWV, a wide linear range of concentration and a low detection limit were obtained for the complementary DNA (miR-141) at the surface of the proposed DNA-biosensor. Using a complementary sequence (miR-141), a remarkable growth was also occurred in the peak current of the MB and decrease of the accumulated HEM, respectively, as compared to the use of a mismatch or a non-complementary sequence. Thus, the suggested DNA-biosensor can be used to identify the miR-141 in early sensitive clinical diagnosis of cancers.

Supplementary Information The online version contains supplementary material available at https://doi.org/10.1007/s00604-022-05301-w.

Acknowledgements This research is a part of Ali Khodadoust's doctoral dissertation. The authors are thankful for all the supports and funding from the Chemical Injuries Research Center and Applied Nano-biotechnology Research Center, Baqiyatallah University of Medical Sciences. Also, the authors are thankful form Islamic Azad University, Yazd Branch, and BioBank, Shiraz University of Medical Sciences, Iran. Authors kindly acknowledge Dr. Amin Ramezani and Dr. Fatemeh Khosravi for their helps.

The research ethics committee of Baqiyatallah University of Medical Sciences has approved the project (Approval ID: IR.BMSU.REC.1398.367).

Declarations

Statements and Declarations The authors declare that they have no known competing financial interests or personal relationships that could have appeared to influence the work reported in this paper.

References

1. Schabath MB, Cote ML (2019) Cancer Progress and Priorities: Lung Cancer. Cancer Epidemiol Biomark Prev 28(10):1563–1579. https://doi.org/10.1158/1055-9965.EPI-19-0221
2. Condrat CE, Thompson DC, Barbu MG, Bugnar OL, Boboc A et al (2020) miRNAs as Biomarkers in Disease: Latest Findings Regarding Their Role in Diagnosis and Prognosis. Cells 9(2):276. https://doi.org/10.3390/cells9020276
3. Gillespie P, Ladame S, O'Hare D (2018) Molecular methods in electrochemical microRNA detection. Analyst 144(1):114–129. https://doi.org/10.1039/c8an01572d
4. Kong YJ, Tan XX, Zhang Y, He QJ, Zhao L et al (2019) MiR-141 promotes cell proliferation and invasion in non-small cell lung cancer by targeting KLF9. Eur Rev Med Pharmacol Sci 23(23):10370–8
5. Zhao Y (2018) The diagnostic and prognostic role of circulating miR-141 expression in non-small-cell lung cancer patients. Int J Clin Exp Pathol 11:2597–2604
6. Tejero R, Navarro A, Campayo M, Viñolas N, Marrades RM et al (2014) miR-141 and miR-200c as Markers of Overall Survival in Early Stage Non-Small Cell Lung Cancer Adenocarcinoma. PLoS ONE 9(7):e101899. https://doi.org/10.1371/journal.pone.0101899
7. Khanmohammadi A, Aghaie A, Vahedi E, Qazvini A, Ghanei M et al (2020) Electrochemical biosensors for the detection of lung cancer biomarkers: A review. Talanta 206:120251. https://doi.org/10.1016/j.talanta.2019.120251
8. Mousavi Nodoushan S, Nasirizadeh N, Amani J, Halabian R, Imani Fooladi AA (2018) An electrochemical aptasensor for Staphylococcal Enterotoxin B detection based on reduced graphene oxide and gold nano-urchins. Biosens Bioelectron 127:221–228. https://doi.org/10.1016/j.bios.2018.12.021
9. Aghili Z, Nasirizadeh N, Divsalar A, Shoeibi S, Yaghmaei P (2018) A highly sensitive miR-195 nanobiosensor for early detection of Parkinson's disease. Artif Cells Nanomed Biotechnol 46(sup1):32–40. https://doi.org/10.1080/21691401.2017.1411930
10. Hu Z, Wang X, Yang Y, Zhao Y, Shen Z et al (2019) MicroRNA expression profiling of lung adenocarcinoma in Xuanwei, China: A preliminary study. Medicine (Baltimore) 98(21):e15717. https://doi.org/10.1097/MD.0000000000015717
11. Aghaei F, Seifati SM, Nasirizadeh N (2017) Development of a DNA biosensor for the detection of phenylketonuria based on a screen-printed gold electrode and hematoxylin. Anal Methods 9(6):966–973. https://doi.org/10.1039/C6AY02853E
12. Golkarieh A-M, Nasirizadeh N, Jahanmardi R (2021) Fabrication of an electrochemical sensor with Au nanorods-graphene oxide hybrid nanocomposites for in situ measurement of cloxacillin. Mater Sci Eng C 118:111317. https://doi.org/10.1016/j.msec.2020.111317
13. Shekari Z, Zare HA-O, Falahati A (2019) Electrochemical sandwich aptasensor for the carcinoembryonic antigen using graphene quantum dots, gold nanoparticles and nitrogen doped graphene modified electrode and exploiting the peroxidase-mimicking activity of a G-quadruplex DNAzyme. Microchim Acta 186:530. https://doi.org/10.1007/s00604-019-3572-9
14. Zhang Q, Li X, Qian C, Dou L, Cui F, Chen X (2018) Label-free electrochemical immunoassay for neuron specific enolase based on 3D macroporous reduced graphene oxide/polyaniline film. Analytical Biochemistry 540–541:1–8. https://doi.org/10.1016/j.ab.2017.10.009
15. Eksin E, Bikkarolla SK, Erdem A, Papakonstantinou P (2018) Chitosan/Nitrogen Doped Reduced Graphene Oxide Modified Biosensor for Impedimetric Detection of microRNA. Electroanalysis 30(3):551–560. https://doi.org/10.1002/elan.201700663
16. Karaboduk K (2019) Electrochemical Determination of Ascorbic Acid Based on AgNPs/PVP-Modified Glassy Carbon Electrode. ChemistrySelect 4:6361–6369. https://doi.org/10.1002/slct.201901102
17. Perumal R, Casale S, de Stefano L, Spadavecchia J (2017) Synthesis and characterization of Ag-Protoporphyrin nano structures using mixed co-polymer method. Front Lab Med 1(2):49–54. https://doi.org/10.1016/j.flm.2017.05.002
18. Asadpour-Zeynali K, Mollarasouli F (2016) Novel electrochemical biosensor based on PVP capped CoFe2O4@CdSe core-shell nanoparticles modified electrode for ultra-trace level determination of rifampicin by square wave adsorptive stripping voltammetry. Biosens Bioelectron 92:509–516. https://doi.org/10.1016/j.bios.2016.10.071
19. Daşdelen Z, yıldız Y, Eriş S, Şen F (2017) Enhanced electrocatalytic activity and durability of Pt nanoparticles decorated on

GO-PVP hybride material for methanol oxidation reaction. Appl Catal B 219:511–516. https://doi.org/10.1016/j.apcatb.2017.08.014
20. Pavinatto A, Mercante LA, Facure MHM, Pena RB, Sanfelice RC et al (2018) Ultrasensitive biosensor based on polyvinylpyrrolidone/chitosan/reduced graphene oxide electrospun nanofibers for 17 alpha - Ethinylestradiol electrochemical detection. Appl Surf Sci 458:431–437. https://doi.org/10.1016/j.apsusc.2018.07.035
21. Yin H, Zhou Y, Zhang H, Meng X, Ai S (2012) Electrochemical determination of microRNA-21 based on graphene, LNA integrated molecular beacon, AuNPs and biotin multifunctional bio bar codes and enzymatic assay system. Biosens Bioelectron 33(1):247–253. https://doi.org/10.1016/j.bios.2012.01.014
22. Wang L, Hua E, Liang M, Ma C, Liu Z et al (2014) Graphene sheets, polyaniline and AuNPs based DNA sensor for electrochemical determination of BCR/ABL fusion gene with functional hairpin probe. Biosens Bioelectron 51:201–207. https://doi.org/10.1016/j.bios.2013.07.049
23. Asadzadeh-Firouzabadi A, Zare HR, Nasirizadeh N (2015) Electrochemical Biosensor for Detection of Target DNA Sequence and Single-Base Mismatch Related to Helicobacter Pylori Using Chlorogenic Acid as Hybridization Indicator. J Electrochem Soc 163(3):B43–B48. https://doi.org/10.1149/2.0461603jes
24. Moazampour M, Zare HR, Shekari Z (2021) Femtomolar determination of an ovarian cancer biomarker (miR-200a) in blood plasma using a label free electrochemical biosensor based on l-cysteine functionalized ZnS quantum dots. Anal Methods 13(17):2021–2029. https://doi.org/10.1039/D1AY00330E
25. Nasirizadeh N, Zare H, Pournaghi-Azar M, Hejazi M (2011) Introduction of hematoxylin as an electroactive label for DNA biosensors and its employment in detection of target DNA sequence and single-base mismatch in human papilloma virus corresponding to oligonucleotide. Biosens Bioelectron 26:2638–2644. https://doi.org/10.1016/j.bios.2010.11.026
26. Xiong X, Huang J, Wang X (2014) DNA Binding Studies of Hematoxylin-Dy(Ш) Complex by Spectrometry Using Acridine Orange as a Probe. Nucleosides, Nucleotides Nucleic Acids 33:730–745. https://doi.org/10.1080/15257770.2014.931589
27. Wang XM, Li HB, Hu YM, Yang DM, Fei D (2007) Study on the interaction between hematoxylin and DNA by spectrometry. Acta Chim Sinica 65:140–146
28. Tian L, Zhang Y, Wang L, Geng Q, Liu D et al (2020) Ratiometric Dual Signal-Enhancing-Based Electrochemical Biosensor for Ultrasensitive Kanamycin Detection. ACS Appl Mater Interfaces 12(47):52713–52720. https://doi.org/10.1021/acsami.0c15898
29. Zhu C, Liu D, Li Y, Shen X, Ma S et al (2020) Ratiometric electrochemical aptasensor for ultrasensitive detection of Ochratoxin A based on a dual signal amplification strategy: Engineering the binding of methylene blue to DNA. Biosens Bioelectron 150:111814. https://doi.org/10.1016/j.bios.2019.111814
30. Panagopoulou MA, Stergiou DV, Roussis IG, Prodromidis MI (2010) Impedimetric Biosensor for the Assessment of the Clotting Activity of Rennet. Anal Chem 82(20):8629–8636. https://doi.org/10.1021/ac1017925
31. Ahlberg S, Antonopulos A, Diendorf J, Dringen R, Epple M et al (2014) PVP-coated, negatively charged silver nanoparticles: A multi-center study of their physicochemical characteristics, cell culture and in vivo experiments. Beilstein J Nanotechnol 5:1944–1965. https://doi.org/10.3762/bjnano.5.205
32. Tian Q, Wang Y, Deng R, Lin L, Liu Y et al (2015) Carbon nanotube enhanced label-free detection of microRNAs based on hairpin probe triggered solid-phase rolling-circle amplification. Nanoscale 7(3):987–993. https://doi.org/10.1039/c4nr05243a
33. Shekari Z, Zare HR, Falahati A (2017) Developing an Impedimetric Aptasensor for Selective Label-Free Detection of CEA as a Cancer Biomarker Based on Gold Nanoparticles Loaded in Functionalized Mesoporous Silica Films. J Electrochem Soc 164(13):B739–B745. https://doi.org/10.1149/2.1991713jes
34. Loaiza ÓA, Campuzano S, López-Berlanga M, Pedrero M, Pingarrón JM (2005) Development of a DNA Sensor Based on Alkanethiol Self- Assembled Monolayer-Modified Electrodes. Sensors 5(6):344–363. https://doi.org/10.3390/s5060344
35. Dehghani M, Nasirizadeh N, Yazdanshenas ME (2019) Determination of cefixime using a novel electrochemical sensor produced with gold nanowires/graphene oxide/electropolymerized molecular imprinted polymer. Mater Sci Eng C 96:654–660. https://doi.org/10.1016/j.msec.2018.12.002.
36. Zhang J, Wang LL, Hou MF, Xia YK, He WH et al (2018) A ratiometric electrochemical biosensor for the exosomal microRNAs detection based on bipedal DNA walkers propelled by locked nucleic acid modified toehold mediate strand displacement reaction. Biosens Bioelectron 102:33–40. https://doi.org/10.1016/j.bios.2017.10.050
37. Cao Z, Duan F, Huang X, Liu Y, Zhou N et al (2019) A multiple aptasensor for ultrasensitive detection of miRNAs by using covalent-organic framework nanowire as platform and shell-encoded gold nanoparticles as signal labels. Anal Chim Acta 1082:176–185. https://doi.org/10.1016/j.aca.2019.07.062
38. Hasanzadeh M, Razmi N, Mokhtarzadeh A, Shadjou N, Mahboob S (2018) Aptamer based assay of plated-derived grow factor in unprocessed human plasma sample and MCF-7 breast cancer cell lysates using gold nanoparticle supported alpha-cyclodextrin. Int J Biol Macromol 108:69–80. https://doi.org/10.1016/j.ijbiomac.2017.11.149
39. Li X, Li X, Li D, Zhao M, Wu H et al (2020) Electrochemical biosensor for ultrasensitive exosomal miRNA analysis by cascade primer exchange reaction and MOF@Pt@MOF nanozyme. Biosens Bioelectron 168:112554. https://doi.org/10.1016/j.bios.2020.112554
40. Daneshpour M, Omidfar K, Ghanbarian H (2016) A novel electrochemical nanobiosensor for the ultrasensitive and specific detection of femtomolar-level gastric cancer biomarker miRNA-106a. Beilstein J Nanotechnol 7:2023–2036. https://doi.org/10.3762/bjnano.7.193
41. Wang Q, Liu Y, Wang X, Wang F, Zhang L, Ge S, Yu J (2021) Ternary Electrochemiluminescence Biosensor Based on DNA Walkers and AuPd Nanomaterials as a Coreaction Accelerator for the Detection of miRNA-141. ACS Applied Materials & Interfaces 13(22):25783–25791. https://doi.org/10.1021/acsami.1c05368
42. Liu L, Yao Y, Ma K, Shangguan C, Jiao S et al (2021) Ultrasensitive photoelectrochemical detection of cancer-related miRNA-141 by carrier recombination inhibition in hierarchical Ti3C2@ReS2. Sens Actuators B Chem 331:129470. https://doi.org/10.1016/j.snb.2021.129470
43. Wang Q, Sun H, Wen D, Wang L, Li L et al (2021) Ultrasensitive electrochemical detection of miRNA based on polymerization signal amplification. Talanta 235:122744. https://doi.org/10.1016/j.talanta.2021.122744
44. Niu X, Lu C, Su D, Wang F, Tan W et al (2021) Construction of a Polarity-Switchable Photoelectrochemical Biosensor for Ultrasensitive Detection of miRNA-141. Anal Chem 93(40):13727–13733. https://doi.org/10.1021/acs.analchem.1c03460
45. Li M-J, An S-Y, Wu Y (2021) Photoelectrochemical monitoring of miRNA based on Au NPs@g-C3N4 coupled with exonuclease-involved target cycle amplification. Anal Chim Acta 1187:339156. https://doi.org/10.1016/j.aca.2021.339156
46. Wu T, Xu T, Chen Y, Yang Y, Xu L-P et al (2018) Renewable superwettable biochip for miRNA detection. Sens Actuators, B Chem 258:715–721. https://doi.org/10.1016/j.snb.2017.11.109

47. Zhou H, Peng J, Qiu X, Gao y, Lu L, Wang W (2017) β-Ni(OH)2 nanosheets: An effective sensing platform for constructing nucleic acid-based optical sensors. J Mater Chem B 5:7426–7432. https://doi.org/10.1039/C7TB01389B
48. Bodulev OL, Sakharov IY (2019) Chemiluminescent Determination of MicroRNA-141 Using Target-Dependent Activation of the Peroxidase-Mimicking DNAzyme. Anal Lett 52(5):813–824. https://doi.org/10.1080/00032719.2018.1498506
49. Jou AF, Lu CH, Ou YC, Wang SS, Hsu SL et al (2015) Diagnosing the miR-141 prostate cancer biomarker using nucleic acid-functionalized CdSe/ZnS QDs and telomerase. Chem Sci 6(1):659–665. https://doi.org/10.1039/c4sc02104e
50. Shi C-X, Li S-X, Chen Z-P, Liu Q, Yu R-Q (2019) Label-Free and Multiplexed Quantification of microRNAs by Mass Spectrometry Based on Duplex-Specific-Nuclease-Assisted Recycling Amplification. Anal Chem 91(3):2120–2127. https://doi.org/10.1021/acs.analchem.8b04583
51. Liu Q, Kang P-J, Chen Z-P, Shi C-X, Chen Y et al (2019) Highly specific and sensitive detection of microRNAs by tandem signal amplification based on duplex-specific nuclease and strand displacement. Chem Commun 55(94):14210–14213. https://doi.org/10.1039/C9CC06790F
52. Su J, Wang D, Nörbel L, Shen J, Zhao Z et al (2017) Multicolor Gold-Silver Nano-Mushrooms as Ready-to-Use SERS Probes for Ultrasensitive and Multiplex DNA/miRNA Detection. Anal Chem 89(4):2531–2538. https://doi.org/10.1021/acs.analchem.6b04729
53. Tran HV, Piro B, Reisberg S, Tran LD, Duc HT et al (2013) Label-free and reagentless electrochemical detection of microRNAs using a conducting polymer nanostructured by carbon nanotubes: Application to prostate cancer biomarker miR-141. Biosens Bioelectron 49:164–169. https://doi.org/10.1016/j.bios.2013.05.007
54. Tran HV, Piro B, Reisberg S, Huy Nguyen L, Dung Nguyen T et al (2014) An electrochemical ELISA-like immunosensor for miRNAs detection based on screen-printed gold electrodes modified with reduced graphene oxide and carbon nanotubes. Biosens Bioelectron 62:25–30. https://doi.org/10.1016/j.bios.2014.06.014
55. Leung W-H, Pang C-C, Pang S-N, Weng S-X, Lin Y-L et al (2021) High-Sensitivity Dual-Probe Detection of Urinary miR-141 in Cancer Patients via a Modified Screen-Printed Carbon Electrode-Based Electrochemical Biosensor. Sensors 21:3183. https://doi.org/10.3390/s21093183
56. Azzouzi S, Fredj Z, Turner APF, Ali MB, Mak WC (2019) Generic Neutravidin Biosensor for Simultaneous Multiplex Detection of MicroRNAs via Electrochemically Encoded Responsive Nanolabels. ACS Sensors 4(2):326–334. https://doi.org/10.1021/acssensors.8b00942
57. Mohammadniaei M, Koyappayil A, Sun Y, Min J, Lee M-H (2020) Gold nanoparticle/MXene for multiple and sensitive detection of oncomiRs based on synergetic signal amplification. Biosens Bioelectron 159:112208. https://doi.org/10.1016/j.bios.2020.112208